

Soft-Landing of Multi-Rotor Drones using a Robust Nonlinear Control and Wind Modeling*

Saeed Rafee Nekoo, Jose Ángel Acosta, Guillermo Heredia and Anibal Ollero

Abstract—Grasping, manipulation, and inspection by multirotor systems require soft landing without any bumps; hence, the one-shot landing subject is critical due to aerodynamics effects under a multirotor unmanned aerial vehicle (UAV). One of the tasks in the HYFLIERS project is landing on a rack of pipes for inspection, mainly measurement of the pipe thickness and corrosion. The rack of pipes generates an unknown disturbance caused by the induced airflow by the propellers during the landing phase. The modeling of this problem is developed for two cases, landing on the ground and rack of pipes. The ground effect modeling is straightforward; however, the rack of pipes imposes more uncertainty on the system modeling. The source of aerodynamics disturbance also could be either external wind or the one caused by the UAV's propellers near the pipes or ground. This work proposes a solution for the one-shot landing of a quadrotor considering the ground effect. First, the induced wind by the rotors near the ground is computed and then the reflection model of that near the ground is defined. Modeling of the quadrotor considering the wind in the environment is done. Next, the reflected wind by the ground is set in the wind model of the system. The uncertainty in the modeling exists due to interference of airflow under the UAV and behavior of that, so a robust nonlinear control is selected to control the system. The correction gain of the sliding mode controller was defined based on the steady-state thrust that plays the role of an upper bound of uncertainty. A simulation has been successfully done to present the advantages of the soft landing method considering the ground effect. The resultant input thrust decreased smoothly near the pipes that compensated the ground effect thrust.

I. INTRODUCTION

Maintenance and inspection of pipes in refineries are necessary tasks in overhauls and during regular checks. The position of the pipes in some cases is out of reach, e.g. see Fig. 1 that a person cannot walk on the pipes to inspect the corrosion and other factors such as the thickness of the pipe. HYFLIERS (HYbrid FLYing-rollIng with-snake-aRm robot for contact inSpection) was defined as a research and innovation action of the EU Horizon 2020 program for aerial robotic inspection in such places to provide a solution [1]. Hybrid aerial robot prototypes that can land on pipes [2] and rack of pipes [3] and move along them have been developed in the project.

Landing over the rack of pipes for setting up the inspection device requires delicate touch down for the safety of the inspection device and avoiding hard contact.



Fig. 1. A sample rack of pipes [4].

A hard contact generates several bumps and endangers the refinery since explosive material runs through the pipes. This research introduces the soft-landing (one-shot landing) approach for multi-rotor drones over a rack of pipes.

Here the mathematical modeling and control are performed in two phases: design based on flat ground for primary assessment and adding the disturbance model to control the landing over the rack of pipes.

The role of the ground effect has been more highlighted in the literature of helicopter control rather than multirotor UAVs. This is extremely difficult for small-scale helicopters since the environment-dependent nature of such a system is strongly effective in control [5]. The ground effect compensation method was used for having a stable flight during take-off and landing [6, 7]. The subject is more critical for small unmanned helicopters since the weight is lower than the big ones and the wind could have been more effective during the take-off and landing. A similar condition is imposed on multirotor UAVs since their weight is kept at a minimum rate. The interference of four or six rotors of the same size

*Research partially supported by the HYFLIERS (H2020-ICT-25-2017-779411) and PILOTING (H2020-ICT-2019-871542) projects funded by the European Union's H2020 programme, and the ARTIC project (RTI2018-102224-B-I00), funded by the Spanish Ministerio de Economía, Industria, y Competitividad.

S. R. Nekoo, J. Á. Acosta, G. Heredia and A. Ollero are with GRVC Robotics Lab., Universidad de Sevilla, Sevilla, Spain; e-mails: saerafee@yahoo.com, {jaar, guiller, aollero}@us.es

makes the aerodynamics effect under the UAV more complex than the helicopters.

The ground effect for a single propeller was reported by Betz [8], and used for helicopter ground effect in forward flight [9]. Sharf et al. presented ground effect experiments and model validation with Draganflyer X8 rotorcraft [10]. It was reported that the ground effect is stronger for multirotor rather than single rotor helicopters. Danjun et al. investigated the autonomous landing of quadrotors based on ground effect modeling [11]. The extension of the image method of Betz was developed and verified experimentally [12]. The practical limit of the ground effect was found at a distance of five radii between the UAV and the ground [12]. The image method of Betz provides a relation for thrusts near the ground as a function of radius of the propellers, total thrust of the rotor and the distance between the UAV and the ground. In this current research, the intention is to find the reflected wind speed, caused by the rotors near the ground based on the image method of Betz. Then the generated wind information will be sent to the generalized model of the quadrotor which consists of a wind gust model.

Wind gust can be modeled as a disturbance force vector in the model [13], or as a wind speed component in the state-space representation of the system [14]. Ambati and Padhi presented the wind gust model for a six-degree-of-freedom (DoF) model of an aircraft [14]. A set of neural networks was employed to learn the unknown sets of the system model and update the system online. Lungu used wind gust modeling based on wind speed for the landing problem of an aircraft based on the backstepping control approach [15].

The main contribution of this work is to combine the generated wind speed, based on the image method of Betz, with the wind speed model (Ref. [15]) to propose a smooth, soft-landing approach for quadrotors. The application is the delivery of the inspection device and soft-landing on the rack of pipes in the refineries. The dangerous site requires extra safety for a landing without bumps and a sudden touchdown.

The rest of the work is structured as follows. Section II expresses quadrotor and wind modeling, ground effect, and computation of induced wind velocity. Section III presents the control design, sliding mode control, and implementation of that on the system. Section IV expresses the simulations. The concluding remarks are summarized in Section V.

II. QUADROTOR AND WIND MODELING

A. Generated wind by a rotor, induced velocity

Consider a propeller to study the momentum theory to find the induced velocity of the airflow passing through one propeller, presented in Fig. 2. Following assumptions must be held for momentum theory [16]:

- The velocity is constant over the disc.
- The pressure is uniform over the disc.
- Rotation imparted to the flow as it passes through the propeller is neglected.
- The flow pass through the propeller can be separated from the rest of the flow by a well-defined stream tube.
- The flow is incompressible.

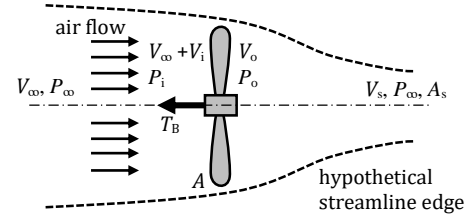


Fig. 2. Application of the momentum theory on a propeller.

The conservation of mass in front and behind the propeller disc results in

$$V_i + V_\infty = V_0, \quad (1)$$

where V (m/s) represents the velocity. Applying Bernoulli's equation for the upstream and downstream line of flow provides:

$$\frac{P_\infty}{\rho} + \frac{V_\infty^2}{2} = \frac{P_i}{\rho} + \frac{(V_\infty + V_i)^2}{2}, \quad (2)$$

$$\frac{P_\infty}{\rho} + \frac{V_s^2}{2} = \frac{P_0}{\rho} + \frac{V_0^2}{2}, \quad (3)$$

where P (Pa) represents pressure and V_s (m/s) is the ultimate downstream velocity of airflow. Substituting (1) into (3) then comparing (2) and (3), results in

$$\Delta P = P_0 - P_i = \frac{1}{2} \rho (V_s^2 - V_\infty^2). \quad (4)$$

The thrust force of the propeller T_B (N) is defined by multiplying (4) into the circular area of the rotating propeller

$$T_B = A \Delta P = \frac{1}{2} \rho A (V_s^2 - V_\infty^2), \quad (5)$$

where ρ (kg/m³) is air density and A (m²) is the generated area by the propeller. On the other hand, the thrust is defined by

$$T_B = \dot{m} (V_s - V_\infty), \quad (6)$$

where \dot{m} (kg/s) is the mass flow rate

$$\dot{m} = \rho A (V_\infty + V_i). \quad (7)$$

Substituting (7) into (6) results in

$$T_B = \rho A (V_\infty + V_i) (V_s - V_\infty). \quad (8)$$

Comparing (5) and (8) provides

$$(V_\infty + V_i) (V_s - V_\infty) = \frac{1}{2} (V_s^2 - V_\infty^2) \Rightarrow V_s = V_\infty + 2V_i,$$

which implies that induced velocity by the propeller is $2V_i$. Rewriting the thrust in terms of induced velocity generates

$$T_B = 2\rho A (V_\infty + V_i) V_i. \quad (9)$$

Solving (9) for V_i provides the induced velocity in terms of thrust [16]:

$$V_i = -\frac{V_\infty}{2} + \sqrt{\frac{V_\infty^2}{4} + \frac{T_B}{2\rho A}}, \quad (10)$$

$$V_0 = \frac{V_\infty}{2} + \sqrt{\frac{V_\infty^2}{4} + \frac{T_B}{2\rho A}}, \quad (11)$$

It should be noted that V_∞ is the airflow speed caused by the wind. In hovering condition without wind, or when the system is flying slowly, V_∞ is set to zero in (10) or (11). In other words, V_0 (m/s) is the generated wind speed by one propeller and its direction is towards the ground when a quadrotor is in hovering condition.

B. Ground effect during landing

The purpose of this section is to define the wind speed caused by the ground effect V_g based on the generated induced velocity of the airflow V_0 from Section II-A. There are two states for flying a quadrotor, far from the ground and near the ground, see Fig. 3. There are three airflow velocities: V_0 the airflow speed far from the ground, V_g the airflow speed near the ground, and the reflection of airflow by the ground V_G .

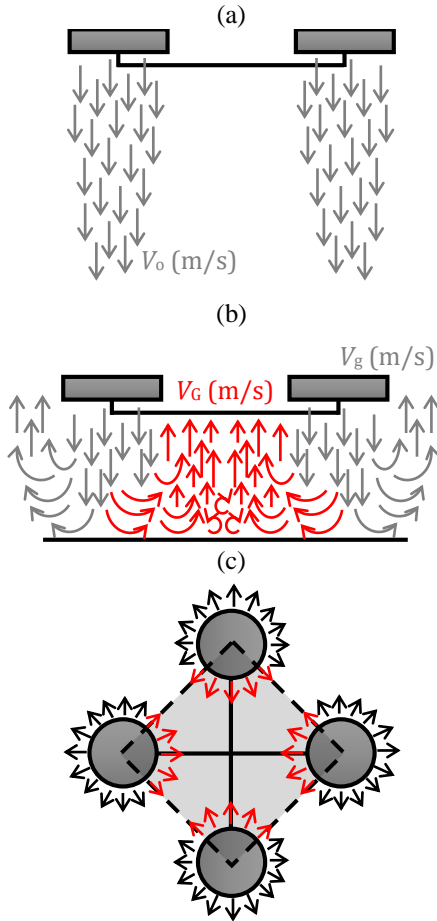


Fig. 3. Illustration of the airflows (a) far from the ground, (b) near the ground; (c) effective area of ground reflection of wind.

The system is free in normal flying far from the ground, presented in Fig. 3(a). In case that the quadrotor approaches the ground two airflows will be built, one flow toward the outside of the system and one airflow toward the inside. Computation of the inward airflow speed, so-called V_G is the objective of this section, Fig. 3(b). The ground effect for propeller systems was proposed to define a relation for

calculating the thrust near the ground based on the image method [8, 9]. The image method of Betz was employed for a single propeller, and then for a quadrotor to verify that experimentally [12]. The relation for a single rotor is [9]:

$$\frac{T_g}{T_B} = \frac{1}{1 - \left(\frac{R}{4z_c}\right)^2}, \quad (12)$$

where T_B (N) is the thrust of the propeller in free flight, T_g (N) is the thrust under the ground effect, R (m) is the radius of the propeller and z_c (m) is the distance of the rotor from the ground. Increasing the number of rotors to four, reforms Eq. (12) to [12]:

$$\frac{T_g}{T_B} = \frac{1}{1 - \left(\frac{R}{4z_c}\right)^2 - \frac{R^2 z_c}{\sqrt{(d + 4z_c^2)^3}} - \frac{R^2 z_c}{2\sqrt{(2d + 4z_c^2)^3}}}. \quad (13)$$

To transform (13) to an equation in terms of airflow velocity, the conversion between force and the mass flow rate is used:

$$T_g = 2\rho A_0 V_g^2, \quad (14)$$

$$T_B = 2\rho A_0 V_0^2, \quad (15)$$

where $A_0 = 4\pi R^2$ (m²) is the area of four propellers. Substituting (14) and (15) in Eq. (13), one could represent the ground reflection of wind with direction towards the ground, $-Z$, which causes the negative sign for V_g :

$$V_g = -V_0 \frac{1}{\sqrt{1 - \left(\frac{R}{4z_c}\right)^2 - \frac{R^2 z_c}{\sqrt{(d + 4z_c^2)^3}} - \frac{R^2 z_c}{2\sqrt{(2d + 4z_c^2)^3}}}}. \quad (16)$$

The *effective* distance between the quadcopter and the ground for studying the ground effect was reported $\text{dist.} = 5R$ [12]. So, if the system is higher than $5R$, the effect of the ground is zero and the UAV flies normally. It can be defined that $V_G(5R) = 0$ and $V_G(0) = V_g$, though the behavior of airflow between the two boundary values is not defined, linear or nonlinear, Fig. 4.

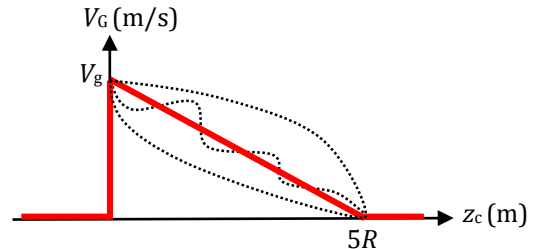


Fig. 4. The ground reflection of wind.

There will be some loss of wind due to the turbulence and interference of the airflows by rotors though the maximum reflection $V_G \leq V_g$ is always less than the V_g . So, the control design based on (16) is safe and covers the ground wind reaction since V_g in reality, is less than the theoretical design. In this research, we assume a linear relation between two

boundary values and present $V_G = -\frac{V_g}{5R}z_c + V_g$ in domain of $z_c \in [0, 5R]$. Based on the direction of the ground reaction, the ultimate airflow speed by the ground is

$$\begin{cases} V_G = \frac{V_g}{5R}z_c - V_g, & z_c \in [0, 5R], \\ 0 & z_c > 5R. \end{cases} \quad (17)$$

Equation (17) implies that the high-speed reaction by the ground is generated near the ground and increases the thrust of the UAV. Landing in this condition faces a couple of bumps before turning off the rotors and removing the thrust. To present a smooth soft landing, without any special landing gear, or better to say one-shot landing, the produced wind reflection by the ground must be considered in the control design and modeling of the system.

For the modeling of the rack of pipes, a disturbance vector is added to demonstrate the uncertain behavior of the reflected wind under the quadrotor, see Fig. 5. The velocity and airflow are a little less than the flat ground due to the escaping airflow around the pipes. This is in favor of the soft-landing; however, the uncertain reflection of the airflow adds uncertainty to the model. For simulation, an uncertain scalar value $V_p = D_p \times [\text{rand}(0,1) - 0.5]$ is added to the model to add the effect of pipes under the system, D_p is amplitude of the uncertainty and $\text{rand}(0,1)$ generates a random disturbance between 0 and 1 (-0.5 shifts the disturbance to zero to have the balance); for the flat ground $D_p = 0$. So, if we have the racks of pipes, Eq. (17) turns into $V_G = \frac{V_g}{5R}z_c - (V_g + V_p)$. In practice, the real airflow under the quadrotor shows its effect and the robust controller compensates the uncertainty in the real landing.

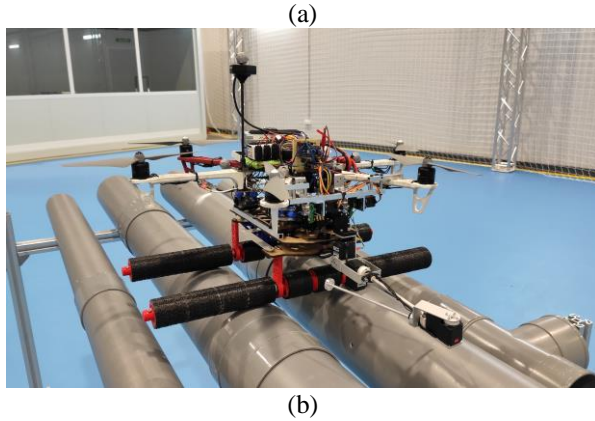


Fig. 5. Reflective induced wind by the propeller over the rack of pipes ((a) quadrotor on a pipe; (b) schematic view).

C. Dynamics of the quadrotor

A moving coordinate (body frame) is attached to the center of mass of the quadrotor defined by $\{x_c, y_c, z_c\}$ that can move and rotate concerning inertial frame $\{X, Y, Z\}$, or Earth frame: Z axis is from the center of the earth to surface, Y axis pointing to the North and X axis pointing to the East. The generalized coordinates include the absolute position of the system and Euler angles for inertial frame $\mathbf{q}(t) = [\xi_1^T(t), \xi_2^T(t)]^T = [x_c(t), y_c(t), z_c(t), \phi(t), \theta(t), \psi(t)]^T$ (m, rad). The angular velocities of the body frame, linear and rotational, are $\mathbf{v}_1(t) = [u(t), v(t), w(t)]^T$ (m/s) and $\mathbf{v}_2(t) = [p(t), q(t), r(t)]^T$ (rad/s) with respect. The kinematics relations between the two reference frames are defined by [17]:

$$\dot{\xi}_1(t) = \mathbf{R}_{ZYX}(\xi_2(t))\mathbf{v}_1(t),$$

$$\dot{\xi}_2(t) = \mathbf{T}(\xi_2(t))\mathbf{v}_2(t),$$

where

$$\mathbf{R}_{ZYX}(\xi_2(t)) = \begin{bmatrix} c_\theta c_\psi & s_\phi s_\theta c_\psi - c_\phi s_\psi & c_\phi s_\theta c_\psi + s_\phi s_\psi \\ c_\theta s_\psi & s_\phi s_\theta s_\psi + c_\phi c_\psi & c_\phi s_\theta s_\psi - s_\phi c_\psi \\ -s_\theta & s_\phi c_\theta & c_\phi c_\theta \end{bmatrix},$$

$$\mathbf{T}(\xi_2(t)) = \begin{bmatrix} 1 & s_\phi t_\theta & c_\phi t_\theta \\ 0 & c_\phi & -s_\phi \\ 0 & s_\phi/c_\theta & c_\phi/c_\theta \end{bmatrix},$$

where i.e. $s_\phi = \sin \phi$. The dynamic model of the quadrotor consists of two translational and rotational parts. The translational dynamics in the body frame is found based on Newton's law $m(\mathbf{v}_2(t) \times \mathbf{v}_1(t) + \dot{\mathbf{v}}_1(t)) = \mathbf{F}_B(t) - m\mathbf{g}\mathbf{R}_{ZYX}^T(\xi_2(t))\mathbf{e}_3$:

$$\dot{\mathbf{v}}_1 = \begin{bmatrix} \dot{u} \\ \dot{v} \\ \dot{w} \end{bmatrix} = \begin{bmatrix} 0 \\ 0 \\ T_B \\ m \end{bmatrix} - \begin{bmatrix} 0 & -r & q \\ r & 0 & -p \\ -q & p & 0 \end{bmatrix} \begin{bmatrix} u \\ v \\ w \end{bmatrix} - g \begin{bmatrix} -s_\theta \\ c_\theta s_\phi \\ c_\theta c_\phi \end{bmatrix},$$

where $\mathbf{e}_3 = [0, 0, 1]^T$, $\mathbf{F}_B(t)$ (N) is the input force vector, $g = 9.81$ (m/s²) gravity acceleration and m (kg) is the total mass of the flying system. Considering hovering condition, the rotation of the body coordinate is negligible concerning the inertial frame; it can be approximated that $\dot{\xi}_1 \approx \mathbf{R}_{ZYX}(\xi_2)\mathbf{v}_1 + \mathbf{R}_{ZYX}(\xi_2)\dot{\mathbf{v}}_1 \approx \dot{\mathbf{v}}_1$ [18], then one could transform the gravity and $\mathbf{F}_B(t)$ into the inertial frame:

$$\dot{\mathbf{v}}_1 = \begin{bmatrix} \dot{u} \\ \dot{v} \\ \dot{w} \end{bmatrix} = \begin{bmatrix} s_\phi s_\psi + c_\phi c_\psi s_\theta \\ s_\phi c_\psi - c_\phi s_\psi s_\theta \\ c_\theta c_\phi \end{bmatrix} \frac{T_B}{m} - \begin{bmatrix} 0 & -r & q \\ r & 0 & -p \\ -q & p & 0 \end{bmatrix} \begin{bmatrix} u \\ v \\ w \end{bmatrix} - \begin{bmatrix} 0 \\ 0 \\ g \end{bmatrix} \quad (18)$$

$$- \frac{1}{m} \begin{bmatrix} D_x & 0 & 0 \\ 0 & D_y & 0 \\ 0 & 0 & D_z \end{bmatrix} \begin{bmatrix} \dot{x}_c \\ \dot{y}_c \\ \dot{z}_c \end{bmatrix},$$

where $\hat{\mathbf{v}}_2(t) = \begin{bmatrix} 0 & -r & q \\ r & 0 & -p \\ -q & p & 0 \end{bmatrix}$, $\mathbf{D} = \text{diag}(D_x, D_y, D_z)$ (kg/s) is the drag coefficient matrix. In other words, Eq. (18) is

considered in the inertial reference frame. The rotational dynamics in the body frame is also $\mathbf{I}\dot{\mathbf{v}}_2(t) + \mathbf{v}_2(t) \times \mathbf{I}\mathbf{v}_2(t) = \boldsymbol{\tau}_B(t)$:

$$\begin{aligned} \dot{\mathbf{v}}_2 &= \begin{bmatrix} \dot{p} \\ \dot{q} \\ \dot{r} \end{bmatrix} \\ &= \begin{bmatrix} \tau_\phi/I_{xx} \\ \tau_\theta/I_{yy} \\ \tau_\psi/I_{zz} \end{bmatrix} \quad (19) \\ -\mathbf{I}^{-1} \begin{bmatrix} 0 & -r & q \\ r & 0 & -p \\ -q & p & 0 \end{bmatrix} \begin{bmatrix} I_{xx} & 0 & 0 \\ 0 & I_{yy} & 0 \\ 0 & 0 & I_{zz} \end{bmatrix} \begin{bmatrix} p \\ q \\ r \end{bmatrix}, \end{aligned}$$

where $\mathbf{I} = \text{diag}(I_{xx}, I_{yy}, I_{zz})$ (kg.m²) is the inertia matrix of the system and $\boldsymbol{\tau}_B(t)$ (N.m) is the input torque vector. Hovering condition also approximates $\dot{\boldsymbol{\xi}}_2 \approx \underbrace{\mathbf{T}(\boldsymbol{\xi}_2)}_0 \mathbf{v}_2 + \underbrace{\mathbf{T}(\boldsymbol{\xi}_2)}_1 \dot{\mathbf{v}}_2 \approx \dot{\mathbf{v}}_2$, then one may consider rotational dynamics Eq. (19), in the inertial frame as well.

The state vector of the system is chosen $\mathbf{x}(t) = [\boldsymbol{\xi}_1^T(t), \boldsymbol{\xi}_2^T(t), \mathbf{v}_1^T(t), \mathbf{v}_2^T(t)]^T$ which results in the state-space representation of dynamics without modeling of wind:

$$\begin{aligned} \dot{\mathbf{x}} &= \begin{bmatrix} \dot{\boldsymbol{\xi}}_1 \\ \dot{\boldsymbol{\xi}}_2 \\ \dot{\mathbf{v}}_1 \\ \dot{\mathbf{v}}_2 \end{bmatrix} \quad (20) \\ &= \begin{bmatrix} \mathbf{R}_{ZYX}(\boldsymbol{\xi}_2)\mathbf{v}_1 \\ \mathbf{T}(\boldsymbol{\xi}_2)\mathbf{v}_2 \\ \mathbf{R}_{ZYX,3}(\boldsymbol{\xi}_2)T_B/m - \hat{\mathbf{v}}_2\mathbf{v}_1 - g\mathbf{e}_3 - \mathbf{D}\dot{\boldsymbol{\xi}}_1/m \\ \mathbf{I}^{-1}(\boldsymbol{\tau}_B - \hat{\mathbf{v}}_2\mathbf{I}\mathbf{v}_2) \end{bmatrix} \end{aligned}$$

The thrust and moment inputs of the quadcopter are produced by four rotors rotating by the angular velocity $\omega_i(t)$ (rad/s). The input limits are the upper bounds of rotors angular velocities and they are expressed by:

$$\boldsymbol{\omega}(t) = \sqrt{\begin{bmatrix} k & k & k & k \\ 0 & -Lk & 0 & Lk \\ -Lk & 0 & Lk & 0 \\ -k_\psi & k_\psi & -k_\psi & k_\psi \end{bmatrix}^{-1} \begin{bmatrix} T_B(t) \\ \tau_\phi(t) \\ \tau_\theta(t) \\ \tau_\psi(t) \end{bmatrix}}$$

where L (m) is the distance between the center of mass of the quadrotor and one rotor, k (Ns²/rad²) is lift constant (thrust factor), and k_ψ (Nms²/rad²) is drag constant.

D. Wind modeling

The input data of the wind in the problem is the wind velocity in inertial coordinates, defined by $\mathbf{W}(t) = [W_x(t), W_y(t), W_z(t)]^T$ (m/s). To transform the wind components to body frame we use the rotation matrix and introduce the wind vector in the body coordinate $\mathbf{W}_c(t) = [W_x(t), W_y(t), W_z(t)]^T = \mathbf{R}_{ZYX}^T(\boldsymbol{\xi}_2(t))\mathbf{W}(t)$ (m/s). The modified form of state-space equation (20) with consideration of wind is [14]:

$$\begin{aligned} \dot{\mathbf{x}} &= \begin{bmatrix} \dot{\boldsymbol{\xi}}_1 \\ \dot{\boldsymbol{\xi}}_2 \\ \dot{\mathbf{v}}_1 \\ \dot{\mathbf{v}}_2 \end{bmatrix} \quad (21) \\ &= \begin{bmatrix} \mathbf{R}_{ZYX}(\boldsymbol{\xi}_2)\mathbf{v}_1 \\ \mathbf{T}(\boldsymbol{\xi}_2)\mathbf{v}_2 \\ \mathbf{R}_{ZYX,3}(\boldsymbol{\xi}_2)T_B/m - \hat{\mathbf{v}}_2(\mathbf{v}_1 + \mathbf{W}_c) - \dot{\mathbf{W}}_c - g\mathbf{e}_3 - \mathbf{D}\dot{\boldsymbol{\xi}}_1/m \\ \mathbf{I}^{-1}(\boldsymbol{\tau}_B - \hat{\mathbf{v}}_2\mathbf{I}\mathbf{v}_2) \end{bmatrix} \end{aligned}$$

where [15]:

$$\dot{\mathbf{W}}_c = \nabla\mathbf{W}_c(\mathbf{v}_1 + \mathbf{W}_c) + \frac{\partial\mathbf{W}_c}{\partial t},$$

in which

$$\begin{aligned} \nabla\mathbf{W}_c &= \mathbf{R}_{ZYX}(\boldsymbol{\xi}_2)\nabla\mathbf{W}\mathbf{R}_{ZYX}^T(\boldsymbol{\xi}_2); \\ \nabla\mathbf{W} &= \begin{bmatrix} \frac{\partial W_x}{\partial x} & \frac{\partial W_y}{\partial x} & \frac{\partial W_z}{\partial x} \\ \frac{\partial W_x}{\partial y} & \frac{\partial W_y}{\partial y} & \frac{\partial W_z}{\partial y} \\ \frac{\partial W_x}{\partial z} & \frac{\partial W_y}{\partial z} & \frac{\partial W_z}{\partial z} \end{bmatrix}. \end{aligned}$$

The embedded wind model in Eq. (21) can be used for general cases and situations. However, in this work, we are interested in improving the almost vertical landing procedure of multirotor UAVs. Specifically, the ground effect must be compensated in the control design to have a one-shot landing (landing without bumps caused by the reflection of the wind by the ground). For this case, the wind vector is defined as $\mathbf{W}(t) = [0, 0, V_G(t)]^T$, where V_G is presented in Eq. (17). It is noted that the modeling is general and could also consider wind in other directions in addition to the one caused by the quadrotors' propellers.

III. CONTROL DESIGN

A. Sliding mode control

The level of uncertainty in this control problem is high due to 1) approximation of reflected wind by the ground as similar as the produced wind by the propellers; 2) approximation of linear behavior of reflected wind between the two boundary conditions; 3) unknown behavior of the wind over the rack of pipes. The uncertainty of the propeller was compensated by neural network modeling [19]; however, here a unified nonlinear controller is proposed. The dynamics of the system are also nonlinear with force coupling between the translational and rotational dynamics. The sliding mode control is proposed, which possesses both robustness and nonlinearity in the design. The sliding mode control offers a nonlinear robust platform to handle the uncertainty in the modeling or caused by external disturbance [20]; the application was also covered a wide range of systems such as unmanned aerial systems [21], tilted motor hexacopter control [22], robotics manipulators [23-25], etc.

Consider a nonlinear system

$$\ddot{\mathbf{q}} = \mathbf{f}(\mathbf{q}, \dot{\mathbf{q}}) + \mathbf{B}(\mathbf{q}, \dot{\mathbf{q}})\mathbf{u},$$

where $\mathbf{q} \in \mathbb{R}^n$ is the generalized coordinates of the system, $\mathbf{u} \in \mathbb{R}^n$ is the generalized input vector of the system (assuming a fully actuated system), $\mathbf{f}(\mathbf{q}, \dot{\mathbf{q}}): \mathbb{R}^n \times \mathbb{R}^n \rightarrow \mathbb{R}^n$ and $\mathbf{B}(\mathbf{q}, \dot{\mathbf{q}}): \mathbb{R}^n \times \mathbb{R}^n \rightarrow \mathbb{R}^{n \times n}$. The error and its derivative are

defined as $\mathbf{e} = \mathbf{q} - \mathbf{q}_{\text{des}}$ and $\dot{\mathbf{e}} = \dot{\mathbf{q}} - \dot{\mathbf{q}}_{\text{des}}$ with respect, in which \mathbf{q}_{des} and $\dot{\mathbf{q}}_{\text{des}}$ are the desired position and velocity of the system.

It should be noted that a quadcopter is under-actuated. This section is dedicated to fully actuated systems; so, the under-actuation compensation of quadcopter control will be done by cascade design in Section III-B.

The sliding surface is set as

$$\mathbf{s} = \dot{\mathbf{e}} + \boldsymbol{\lambda}\mathbf{e}, \quad (22)$$

where $\boldsymbol{\lambda} \in \mathbb{R}^{n \times n}$ is a strictly positive matrix. The objective is to find a controller to regulate the generalized coordinates towards the sliding surface and keep them on the surface. The sliding condition is [20]:

$$\frac{1}{2} \frac{d}{dt} s_i^2 \leq -\eta_i |s_i|, \text{ for } i = 1, \dots, n, \quad (23)$$

where η_i is a strictly positive constant. Solving $\dot{\mathbf{s}} = \mathbf{0}$ from Eq. (22) provides the equivalent control law, responsible for keeping the states on the sliding surface:

$$\mathbf{u}_n = \mathbf{B}^{-1}(\mathbf{q}, \dot{\mathbf{q}})(\dot{\mathbf{q}}_{\text{des}} - \mathbf{f}(\mathbf{q}, \dot{\mathbf{q}}) - \boldsymbol{\lambda}\dot{\mathbf{e}}). \quad (24)$$

In general, the exact values of $\mathbf{f}(\mathbf{q}, \dot{\mathbf{q}})$ and $\mathbf{B}(\mathbf{q}, \dot{\mathbf{q}})$ are not known and states are not on the sliding surface. Hence, a correction term:

$$\mathbf{u}_c = -\mathbf{K}(\mathbf{q}, \dot{\mathbf{q}})\text{sign}(\mathbf{s}),$$

is added to (24) for completing the control law:

$$\begin{aligned} \mathbf{u} &= \mathbf{u}_n + \mathbf{u}_c \\ &= \mathbf{B}^{-1}(\mathbf{q}, \dot{\mathbf{q}})(\dot{\mathbf{q}}_{\text{des}} - \bar{\mathbf{f}}(\mathbf{q}, \dot{\mathbf{q}}) - \boldsymbol{\lambda}\dot{\mathbf{e}}) - \mathbf{K}(\mathbf{q}, \dot{\mathbf{q}})\text{sign}(\mathbf{s}), \end{aligned}$$

where $\mathbf{K}(\mathbf{q}, \dot{\mathbf{q}}): \mathbb{R}^n \times \mathbb{R}^n \rightarrow \mathbb{R}^{n \times n}$ is the correction gain, $\underline{\mathbf{B}}(\mathbf{q}, \dot{\mathbf{q}})$ is the lower bound of $\mathbf{B}(\mathbf{q}, \dot{\mathbf{q}})$ and $\bar{\mathbf{f}}(\mathbf{q}, \dot{\mathbf{q}})$ is the upper bound of $\mathbf{f}(\mathbf{q}, \dot{\mathbf{q}})$. It should be noted that to remove the negative effects of chattering, saturation function $\text{sat}(\cdot)$ could be employed instead of $\text{sign}(\cdot)$.

B. Implementation on a quadcopter: Translational and rotational control

Quadrotors are under-actuated systems due to a lack of inputs for XY planar motion in translational dynamics. To present a six-degree-of-freedom controller, a cascade design was used [26]. With the cascade design, two translational and orientation control were designed.

The relevant row of $\dot{\mathbf{v}}_1$ in (21) presents the translational dynamics of the system, based on that the elements of control law are chosen:

$$\begin{aligned} \mathbf{F}_t &= \mathbf{B}_t^{-1}(\dot{\mathbf{q}}_{t,\text{des}} - \bar{\mathbf{f}}_t(\mathbf{q}, \dot{\mathbf{q}}) - \boldsymbol{\lambda}_t \dot{\mathbf{e}}_t) - \mathbf{K}_t(\mathbf{q}, \dot{\mathbf{q}})\text{sign}(\mathbf{s}_t), \\ \mathbf{B}_t &= 1/m\mathbf{I}_{3 \times 3}, \end{aligned} \quad (25)$$

$$\bar{\mathbf{f}}_t(\mathbf{q}, \dot{\mathbf{q}}) = -\hat{\mathbf{v}}_2(\mathbf{v}_1 + \bar{\mathbf{W}}_c) - \dot{\bar{\mathbf{W}}}_c - g\mathbf{e}_3 - \mathbf{D}\dot{\boldsymbol{\xi}}_1/m, \quad (25)$$

where $\mathbf{F}_t \in \mathbb{R}^3$ is a control input vector with the assumption of having a fully actuated system, $\bar{\mathbf{W}}_c$ and $\dot{\bar{\mathbf{W}}}_c$ are the estimated bound of wind vector and its velocity near the ground or pipes; their actual values are unknown. The error vector and its

velocity are also $\mathbf{e}_t = \boldsymbol{\xi}_1 - \boldsymbol{\xi}_{1,\text{des}}$ and $\dot{\mathbf{e}}_t = \dot{\boldsymbol{\xi}}_1 - \dot{\boldsymbol{\xi}}_{1,\text{des}}$ with respect. The cascade approach transforms the three inputs of the translation dynamics into one total thrust [27]:

$$\begin{aligned} T_B &= m\{[\mathbf{R}_{ZYX,3}(\boldsymbol{\xi}_2)]_1 F_{t,1} + [\mathbf{R}_{ZYX,3}(\boldsymbol{\xi}_2)]_2 F_{t,2} \\ &\quad + [\mathbf{R}_{ZYX,3}(\boldsymbol{\xi}_2)]_3 (F_{t,3} + g)\}. \end{aligned}$$

Definition of $\bar{\mathbf{W}}_c$ in (25) is based on the steady-state value of thrust

$$T_{B,ss} = c_1 mg, \quad (26)$$

where $c_1 > 1$ is chosen to dominate the \mathbf{W}_c in the actual

system. Hence, $\bar{V}_0 = -\sqrt{\frac{T_{B,ss}}{2\rho A_0}}$, $\bar{V}_G = \frac{\bar{V}_g}{5R} z_c - (\bar{V}_g + \bar{V}_p)$ and the rest of the derivation of the wind model is based on Section II-B. The bound of uncertainty due to the shape of the pipes ($\bar{V}_p = D_p$) is set in the control law to compensate for the disturbance. In real flights, tuning \bar{V}_p provides a robust controller for smooth landing without having exact information about the geometry of the rack of the pipes under the UAV. Other parameters are defined as $\bar{\mathbf{W}} = [0, 0, \bar{V}_G]^T$, $\frac{\partial \bar{\mathbf{W}}_c}{\partial t} = \mathbf{0}$, and

$$\begin{aligned} &\frac{\partial W_z}{\partial z} \\ &= -V_0 \frac{\partial}{\partial z} \frac{1}{\sqrt{1 - \left(\frac{R}{4z_c}\right)^2 - \frac{R^2 z_c}{\sqrt{(d + 4z_c^2)^3}} - \frac{R^2 z_c}{2\sqrt{(2d + 4z_c^2)^3}}}} \end{aligned}$$

The rotational dynamics is the relevant row of $\dot{\mathbf{v}}_2$ in (21) that provides

$$\boldsymbol{\tau}_B = \mathbf{B}_0^{-1}(\dot{\mathbf{q}}_{0,\text{des}} - \mathbf{f}_0(\mathbf{q}, \dot{\mathbf{q}}) - \boldsymbol{\lambda}_0 \dot{\mathbf{e}}_0) - \mathbf{K}_0(\mathbf{q}, \dot{\mathbf{q}})\text{sign}(\mathbf{s}_0),$$

$$\mathbf{B}_0 = \mathbf{I}^{-1},$$

$$\mathbf{f}_0(\mathbf{q}, \dot{\mathbf{q}}) = -\mathbf{I}^{-1}\hat{\mathbf{v}}_2 \mathbf{I} \mathbf{v}_2,$$

where $\mathbf{e}_0 = \boldsymbol{\xi}_2 - \boldsymbol{\xi}_{2,\text{des}}$ and $\dot{\mathbf{e}}_0 = \dot{\boldsymbol{\xi}}_2 - \dot{\boldsymbol{\xi}}_{2,\text{des}}$. The definition of the desired orientation is based on cascade design [27].

To define the SMC gain of the translational control, one could use the sliding condition (23):

$$\mathbf{s}_t^T \dot{\mathbf{s}}_t \leq -\boldsymbol{\eta}^T |\mathbf{s}_t|,$$

which results in

$$\mathbf{s}_t^T (\mathbf{f}_t - \bar{\mathbf{f}}_t - \mathbf{K}_t \text{sign}(\mathbf{s}_t)) \leq -\boldsymbol{\eta}^T |\mathbf{s}_t|. \quad (27)$$

Considering that in regulation $\dot{\mathbf{q}}_{t,\text{des}} = \mathbf{0}$, and substituting the \mathbf{f}_t from (21) and $\bar{\mathbf{f}}_t$ from (25) into (27) results in

$$\begin{aligned} \mathbf{s}_t^T (\hat{\mathbf{v}}_2(\bar{\mathbf{W}}_c - \mathbf{W}_c) + \dot{\bar{\mathbf{W}}}_c - \dot{\mathbf{W}}_c - \mathbf{K}_t \text{sign}(\mathbf{s}_t)) \\ \leq -\boldsymbol{\eta}^T |\mathbf{s}_t|. \end{aligned} \quad (28)$$

Rewriting (28) as $\mathbf{s}_t^T (\boldsymbol{\delta} - \mathbf{K}_t \text{sign}(\mathbf{s}_t)) \leq -\boldsymbol{\eta}^T |\mathbf{s}_t|$ where $\boldsymbol{\delta} = \hat{\mathbf{v}}_2(\bar{\mathbf{W}}_c - \mathbf{W}_c) + \dot{\bar{\mathbf{W}}}_c - \dot{\mathbf{W}}_c$, represents the scalar form of that:

$$\sum_{i=1}^3 s_{t,i} \delta_i - \sum_{i=1}^3 \sum_{j=1}^3 s_{t,i} K_{t,ij} \text{sign}(s_{t,j}) \leq - \sum_{i=1}^3 \eta_i |s_{t,i}|. \quad (29)$$

Dividing Eq. (29) by $s_{t,i}$ removes the summation for i and presents

$$\begin{aligned} \delta_i - \sum_{j=1}^3 K_{t,ij} \text{sign}(s_{t,j}) &\leq -\eta_i \frac{|s_{t,i}|}{s_{t,i}} \\ \Rightarrow \delta_i - \sum_{j=1}^3 K_{t,ij} \text{sign}(s_{t,j}) &\leq -\eta_i \text{sign}(s_{t,i}). \end{aligned} \quad (30)$$

Computing the absolute value of (30) and considering a diagonal correction gain $[K_{t,ij} = 0]_{i \neq j}$, one could express

$$|K_{t,ii}| \geq \eta_i + |\delta_i|,$$

which can be represented in matrix form

$$\tilde{\mathbf{K}}_t \geq \boldsymbol{\eta} + \left| \hat{\mathbf{v}}_2(\bar{\mathbf{W}}_c - \mathbf{w}_c) + \dot{\bar{\mathbf{w}}}_c - \dot{\mathbf{w}}_c \right|, \quad (31)$$

Consequently, the ultimate correction gain is

$$\mathbf{K}_t(\mathbf{q}, \dot{\mathbf{q}}) = \text{diag} \left(\tilde{K}_{t,11}(\mathbf{q}, \dot{\mathbf{q}}), \tilde{K}_{t,22}(\mathbf{q}, \dot{\mathbf{q}}), \tilde{K}_{t,33}(\mathbf{q}, \dot{\mathbf{q}}) \right). \quad (32)$$

IV. SIMULATIONS

A quadrotor is considered for simulation for point-to-point motion (regulation case) in a limited finite time. The total mass of the system is $m = 1.2$ (kg), drag coefficients are $D_{ii} = 0.25$ (kg/s) for $i = 1, 2, 3$; $L = 0.225$ (m), the radius of the propellers are $R = 0.075$ (m), moment of inertia of the UAV is $I_{xx} = 7 \times 10^{-3}$, $I_{yy} = 7.3 \times 10^{-3}$, $I_{zz} = 3.3 \times 10^{-3}$ (kgm²), lift constant is $k = 2.98 \times 10^{-5}$ (Ns²/rad²), the drag coefficient is $k_{\psi} = 1.14 \times 10^{-6}$ (Nms²/rad²) and $\rho = 1.225$ (kg/m³). The modeling of the quadcopter and the wind have been presented for a general regulation problem. However, the research intends to study the soft-landing subject. Based on this scenario, the initial condition is selected far from the ground on an arbitrary point $\xi_1(0) = [1, -1.5, 19.25]^T$ (m), and the final position of the system is on the ground, $z_c(t_f) = 0$. Without loss of generality, equilibrium is selected for the final position $\xi_1(t_f) = [0, 0, 0]^T$ (m). The initial and final orientation is also set to zero.

The control gains are selected as $\boldsymbol{\lambda}_t = 0.2 \times \mathbf{I}_{3 \times 3}$, $\boldsymbol{\lambda}_o = 0.5 \times \mathbf{I}_{3 \times 3}$ and $\mathbf{K}_o = 0.1 \times \mathbf{I}_{3 \times 3}$. The correction gain of translation control is defined by Eqs. (31) and (32) in which $\boldsymbol{\eta} = [1, 1, 1]^T$. The scaling factor is also set $c_1 = 1.1$ in Eq. (26). The time of simulation was set 50s though it should be noted that when the UAV lands on the ground, the control loop is finished. So, the final time of the simulation is defined by the control loop when the quadrotor lands at $z_c(t_f) = 0$; for this simulation the final time was gained around 20s.

The position variables of the quadrotor are illustrated in Fig. 6. The velocity of the system is depicted in Fig. 7, which shows the Z component possessed negative velocity near the

ground and caused deceleration. The reflection of wind by the ground is shown in Fig. 8. The produced wind by the rotors is plotted in Fig. 9. The total thrust of the system is presented in Fig. 10 and the angular velocities of the rotors in Fig. 11. In both graphs, it is clear that instead of a constant steady-state value for thrust or angular velocities of the rotors, we have a jump and sudden smooth decrease in the values which show the ground effect. This confirms that near the landing, less thrust is needed and the ground provides extra thrusts for the UAV.

Due to less need to thrust in the system based on the ground effect in the control design, the system goes (smoothly) to the negative zone of the Z-axis and is regulated to a small negative error in simulation. The cause of the small negative error is that the function in (13) is defined based on positive z_c . So, a condition (a switch) has been designed to stop the simulation when the UAV is landed.

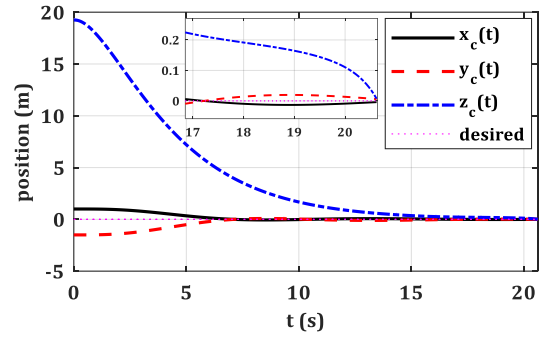


Fig. 6. Position variables of the quadrotor.

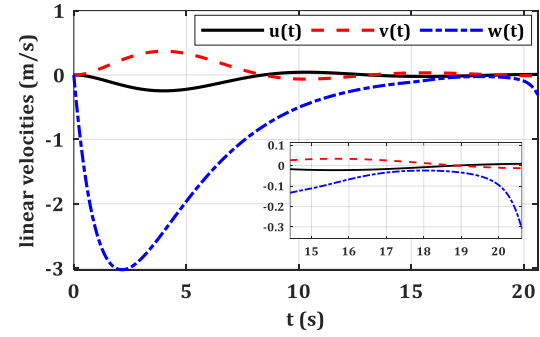


Fig. 7. The velocity of the system in regulation.

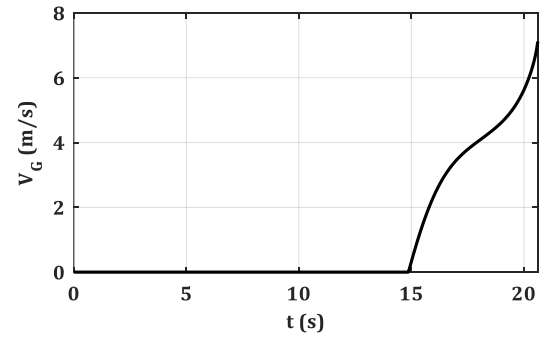


Fig. 8. Reflection of wind by the ground.

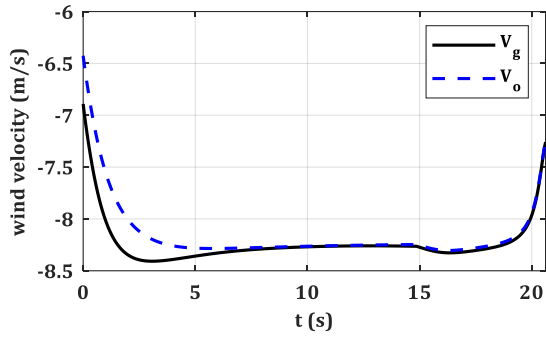


Fig. 9. Induced velocity near and far from the ground.

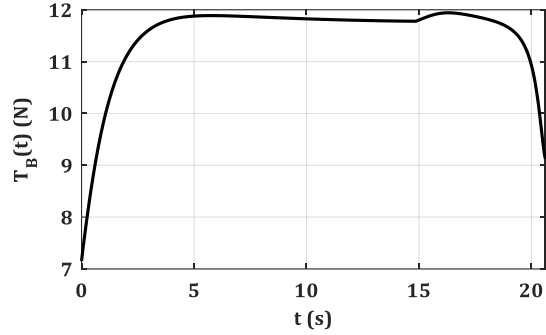


Fig. 10. The thrust of the system.

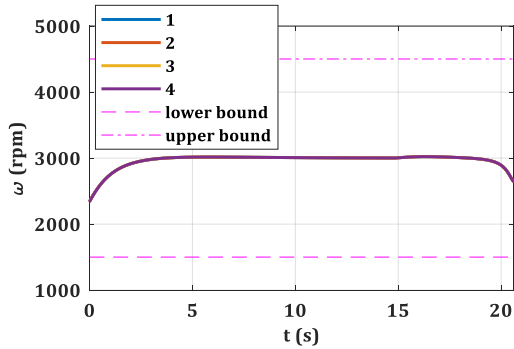


Fig. 11. Angular velocities of the rotors.

The time of landing is interchangeable by the control parameter λ_t . A series of simulations for $\lambda_t = \{0.06, 0.12, 0.18, 0.24, 0.3\}$ has been performed to demonstrate the effect of the control parameter on the landing time, Fig. 12. The decrease in landing time requires more force, to land faster, though the force should be reduced from the thrust to have a controlled fall, Fig. 13.

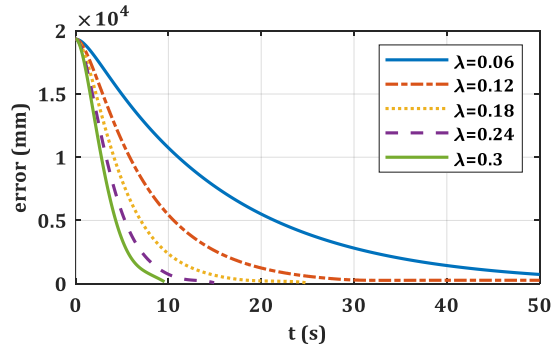


Fig. 12. Effect of λ_t on the final time of landing.

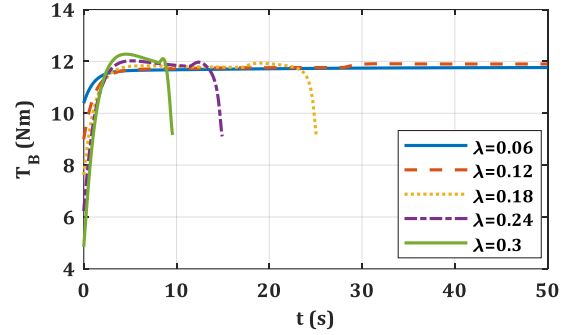


Fig. 13. Effect of λ_t on total thrust.

Soft-landing over the racks of pipes: The previous simulation verified the capability of the proposed wind modeling approach for soft-landing considering the ground effect. To show the main achievement of the research, landing over racks of pipes, the amplitude of disturbance due to the pipes is set $D_p = 0.1$; and the reflected wind speed is shown in Fig. 14. The error increased to 15.8mm as well. The simulation showed that the uncertainty due to the shape of the pipes can be handled by the robust nonlinear controller. The rest of the results were almost similar to landing on flat ground with a little bit more 5mm error.

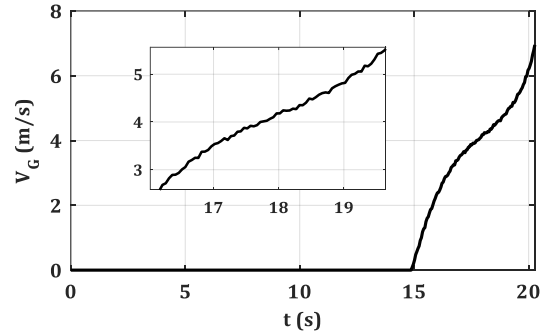


Fig. 14. The ground effect with disturbance of the rack of pipes.

Practical implementation: For practical implementation, the random parameters for generating uncertainty in the model are removed and the actual shape of the pipes plays the role of disturbance. In case there is a controlled quadcopter with two translation and orientation control, the minimum required changes for having a soft-landing controller without physical modification is to use

$$\mathbf{F}_t = \mathbf{B}_t^{-1}(\dot{\mathbf{q}}_{t,des} - \bar{\mathbf{f}}_t(\mathbf{q}, \dot{\mathbf{q}}) - \lambda_t \dot{\mathbf{e}}_t) - \mathbf{K}_t(\mathbf{q}, \dot{\mathbf{q}})\text{sign}(\mathbf{s}_t),$$

where

$$\bar{\mathbf{f}}_t(\mathbf{q}, \dot{\mathbf{q}}) = -\hat{\mathbf{v}}_2(\mathbf{v}_1 + \bar{\mathbf{W}}_c) - \dot{\bar{\mathbf{W}}}_c - g\mathbf{e}_3 - \mathbf{D}\dot{\xi}_1/m,$$

includes the upper bound of translation dynamics and

$$\mathbf{K}_t(\mathbf{q}, \dot{\mathbf{q}}) = \text{diag}(\tilde{\mathbf{K}}_{t,11}(\mathbf{q}, \dot{\mathbf{q}}), \tilde{\mathbf{K}}_{t,22}(\mathbf{q}, \dot{\mathbf{q}}), \tilde{\mathbf{K}}_{t,33}(\mathbf{q}, \dot{\mathbf{q}})),$$

is the correction gain in which $\tilde{\mathbf{K}}_t > \boldsymbol{\eta} + |\hat{\mathbf{v}}_2(\bar{\mathbf{W}}_c - \mathbf{W}_c) + \dot{\bar{\mathbf{W}}}_c - \dot{\mathbf{W}}_c|$. The robustness of the design is incorporated through $\bar{\mathbf{W}}_c$ and $\dot{\bar{\mathbf{W}}}_c$ in both correction gain and upper bound of translation dynamics $\bar{\mathbf{f}}_t(\mathbf{q}, \dot{\mathbf{q}})$. The tuning is also setting the parameters of λ_t and D_p .

V. CONCLUSIONS

This work presented a control approach for the soft landing of a quadcopter without adding a physical soft landing gear. The produced reflected wind by the rotors near the ground generates extra thrust for the system and deviates that from a predefined trajectory for a smooth landing. A couple of bumps usually happen without consideration of the ground effect. The generated induced thrust and wind velocity from the rotors have been calculated and modeled. The reflection of the wind from the ground is effective in a limited distance which is considered in this work. The ultimately reflected wind modeled in the dynamics of the system. The landing over the rack of pipes was considered in the model and simulation. There is uncertainty in the modeling and behavior of the wind through the boundary values are defined. Proposing a robust nonlinear control for covering the uncertainty, the model successfully controlled. The correction gain of the sliding mode controller was adaptively set based on the steady-state value of thrust and wind. The simulation showed that thrust should be reduced near the landing since extra thrust is generated by the ground effect. The results confirmed the expected landing behavior and acceptable precision without bumping and overshoot.

ACKNOWLEDGMENTS

This work has been partially supported by the HYFLIERS (H2020-ICT-25-2017-779411) and PILOTING (H2020-ICT-2019-871542) projects funded by the European Union's H2020 Programme, and the ARTIC project (RTI2018-102224-B-I00), funded by the Spanish Ministerio de Economía, Industria, y Competitividad.

REFERENCES

- [1] <https://www.oulu.fi/hyfliders/>.
- [2] A. Lopez-Lora, P. J. Sanchez-Cuevas, A. Suarez, A. Garofano, A. Ollero, and G. Heredia, "MHYRO: Modular HYbrid RObot for contact inspection and maintenance in oil&gas plants," in *IEEE/RSJ International Conference on Intelligent Robots and Systems (IROS)*, Nevada, Las Vegas, 2020.
- [3] A. Suarez, A. Caballero, A. Garofano, P. J. Sanchez-Cuevas, G. Heredia, and A. Ollero, "Aerial Manipulator With Rolling Base for Inspection of Pipe Arrays," *IEEE Access*, vol. 8, pp. 162516-162532, 2020.
- [4] <https://www.theprocesspiping.com/>.
- [5] R. Mahony and T. Hamel, "Adaptive compensation of aerodynamic effects during takeoff and landing manoeuvres for a scale model autonomous helicopter," *European Journal of Control*, vol. 7, pp. 43-57, 2001.
- [6] K. Nonaka and H. Sugizaki, "Integral sliding mode altitude control for a small model helicopter with ground effect compensation," in *Proceedings of the 2011 American Control Conference*, San Francisco, CA, USA, 2011, pp. 202-207.
- [7] T. K. Roy, M. Garratt, H. R. Pota, and M. K. Samal, "Robust altitude control for a small helicopter by considering the ground effect compensation," in *Proceedings of the 10th World Congress on Intelligent Control and Automation*, Beijing, China, 2012, pp. 1796-1800.
- [8] A. Betz, "The ground effect on lifting propellers," *Technical Memorandums, National Advisory Committee for Aeronautics, N. 836*, 1937.
- [9] I. C. Cheeseman and W. E. Bennett, "The effect of the helicopter rotor by ground on a forward flight," *Aeronautical Research Council Reports and Memoranda, No. 3021*, 1957.
- [10] I. Sharf, M. Nahon, A. Harmat, W. Khan, M. Michini, N. Speal, *et al.*, "Ground effect experiments and model validation with Draganflyer X8 rotorcraft," in *2014 International Conference on Unmanned Aircraft Systems (ICUAS)*, Orlando, FL, USA, 2014, pp. 1158-1166.
- [11] L. Danjun, Z. Yan, S. Zongying, and L. Geng, "Autonomous landing of quadrotor based on ground effect modelling," in *2015 34th Chinese Control Conference (CCC)*, Hangzhou, China, 2015, pp. 5647-5652.
- [12] P. Sanchez-Cuevas, G. Heredia, and A. Ollero, "Characterization of the aerodynamic ground effect and its influence in multicopter control," *International Journal of Aerospace Engineering*, vol. 2017, 2017.
- [13] N. K. Tran, E. Bulka, and M. Nahon, "Quadrotor control in a wind field," in *International Conference on Unmanned Aircraft Systems*, Colorado, USA, 2015, pp. 320-328.
- [14] P. R. Ambati and R. Padhi, "A neuro-adaptive augmented dynamic inversion design for robust auto-landing," *IFAC Proceedings Volumes*, vol. 47, pp. 12202-12207, 2014.
- [15] M. Lungu, "Backstepping and dynamic inversion combined controller for auto-landing of fixed wing UAVs," *Aerospace Science and Technology*, vol. 96, p. 105526, 2020.
- [16] B. W. McCormick, "Aerodynamics Aeronautics and Flight Mechanics," 2nd ed. New York NY: John Wiley & Sons Inc, 1995.
- [17] S. R. Nekoo, J. Á. Acosta, A. E. Gomez-Tamm, and A. Ollero, "Optimized thrust allocation of variable-pitch propellers quadrotor control: A comparative study on flip maneuver," in *2019 Workshop on Research, Education and Development of Unmanned Aerial Systems (RED UAS)*, Cranfield, United Kingdom, United Kingdom, 2019, pp. 86-95.
- [18] S. R. Nekoo, J. Á. Acosta, and A. Ollero, "Collision Avoidance of SDRE Controller using Artificial Potential Field Method: Application to Aerial Robotics," in *2020 International Conference on Unmanned Aircraft Systems (ICUAS)*, Athens, Greece, 2020, pp. 551-556.
- [19] H. Tourajzadeh, S. Manteghi, and S. Nekoo, "Numerical and neural network modeling and control of an aircraft propeller," *Journal of Computational Applied Mechanics*, vol. 49, pp. 63-69, 2018.
- [20] J.-J. E. Slotine and W. Li, *Applied nonlinear control* vol. 199: prentice-Hall Englewood Cliffs, NJ, 1991.

Preprint version of:

Nekoo, S. R., Acosta, J. Á., Heredia, G. & Ollero, A. (2021). Soft-Landing of Multi-Rotor Drones using a Robust Nonlinear Control and Wind Modeling. *The 2021 International Conference on Unmanned Aircraft Systems*

- [21] C. Rosales, J. Gimenez, F. Rossomando, C. Soria, M. Sarcinelli-Filho, and R. Carelli, "UAVs formation control with dynamic compensation using Neuro adaptive SMC," in *2019 international conference on unmanned aircraft systems (ICUAS)*, Atlanta, GA, USA, 2019, pp. 93-99.
- [22] J. M. Arizaga, H. Castañeda, and P. Castillo, "Adaptive control for a tilted-motors hexacopter UAS flying on a perturbed environment," in *2019 International Conference on Unmanned Aircraft Systems (ICUAS)*, Atlanta, GA, USA, 2019, pp. 171-177.
- [23] R. Shiri, S. Rafee Nekoo, M. Habibnejad Korayem, and S. Kazemi, "Finite-time nonsingular terminal sliding mode control: A time setting approach," *Proceedings of the Institution of Mechanical Engineers, Part I: Journal of Systems and Control Engineering*, vol. 233, pp. 1392-1412, 2019.
- [24] N. Y. Lademakhi, R. Shiri, A. Korayem, S. Nekoo, and Z. Fazilati, "Superiority of finite time SDRE and non-singular terminal SMC controller for n-DOF manipulators," in *2018 6th RSI International Conference on Robotics and Mechatronics (IcRoM)*, Tehran, Iran, 2018, pp. 315-321.
- [25] Z. Zhou and B. Wu, "Adaptive sliding mode control of manipulators based on fuzzy random vector function links for friction compensation," *Optik*, vol. 227, p. 166055, 2021.
- [26] Z. Zuo, "Trajectory tracking control design with command-filtered compensation for a quadrotor," *IET control theory & applications*, vol. 4, pp. 2343-2355, 2010.
- [27] S. R. Nekoo, J. Á. Acosta, and A. Ollero, "Fully coupled six-DoF nonlinear suboptimal control of a quadrotor: Application to variable-pitch rotor design," in *Iberian Robotics conference*, 2019, pp. 72-83.